J|A|C|S
ARTICLES
Published on Web 11/19/2003

Ureases: Quantum Chemical Calculations on Cluster Models

Dimas Suárez,[†] Natalia Díaz,[†,§] and Kenneth M. Merz, Jr.*[,‡]

Contribution from the Departamento de Química Física y Analítica, Universidad de Oviedo, C/ Julián Clavería 8, 33006 Oviedo, Asturias, Spain and Department of Chemistry, The Pennsylvania State University, 152 Davey Laboratory, University Park, Pennsylvania 16802-6300

Received March 3, 2003; E-mail: merz@psu.edu

Abstract: Herein, we present results from a computational study of dinickel complexes that are relevant to the catalytic hydrolysis of urea exerted by the urease enzymes. The B3LYP density functional is used to characterize the equilibrium geometry, electronic and magnetic properties, and energies for a series of realistic complexes modeling the active site of ureases. The analysis of the theoretical results gives new insight into the structure, substrate binding, and catalytic mechanism. The water bridge between the two Ni(II) ions observed in the crystallographic structures of the ureases was assigned to a hydroxide bridge in agreement with the observed small antiferromagnetic coupling. Both monodentate and bidentate urea-bound complexes, in which urea had favorable orientations for catalysis, were characterized. Finally, two reaction mechanisms were investigated starting from the monodetante and bidentate urea-bound complexes, respectively. Both a Ni1···Ni2 bridging hydroxide and a Ni2-bound water molecule play crucial roles in the two mechanisms.

Introduction

Urea is formed in large quantities as a product of catabolism of nitrogen-containing compounds. Owing to its resonance stabilization, urea is highly stable in aqueous solutions. For example, urea spontaneously eliminates ammonia to form cyanic acid with a half-life of 3.6 years at 38°C. To avoid the accumulation of urea, the enzyme urease,[1] which is present in a variety of plants, selected fungi, and a broad range of bacterial species, hydrolyzes urea to give ammonia and carbamate 10^{14} times faster[2] than the uncatalyzed elimination of urea to yield ammonia and cyanic acid (see Scheme 1).

The enzymatic hydrolysis of urea causes an abrupt overall pH increase, which results in negative side effects for both human and animal health and for agriculture. On one hand, the widespread activity of urease in soil, present both in living ureolytic bacteria and as extracellular urease, can severely decrease the efficiency of urea as a soil fertilizer and simultaneously release large quantities of toxic ammonia. On the other hand, urease activity constitutes a virulence factor in human and animal infections of the urinary and gastrointestinal tracts. In particular, *Helicobacter pylori*,[3,4] an etiologic bacteria present in a variety of gastroduodenal diseases including cancer, produces a large amount of urease which is believed to play an essential role in facilitating the survival of the *H. pylori* bacteria. Understanding the catalytic machinery of this enzyme will be crucial for the design of new inhibitors targeted against ureases in order to eliminate the negative side effects of the activity of this enzyme on humans and on the environment.

Scheme 1

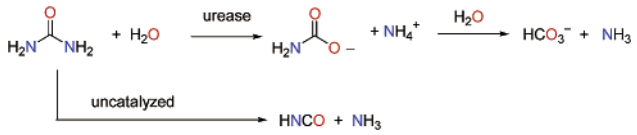

Coordination Chemistry of the Catalytic Nickel Ions in the Ureases. Urease represents a milestone in biological inorganic chemistry because it was the first enzyme to be crystallized (1926) and the first metalloenzyme characterized as a nickel-containing enzyme (1975). Five other important enzymes that depend on nickel for activity have been identified, although they catalyze different reactions with the nickel centers in different coordination environments.[5] For the ureases, their amino acid sequences are highly conserved, and the constant presence of nickel ions in the active site suggests a common catalytic pathway.[1,6]

According to X-ray absorption spectroscopy (XAS) data, urease contains two pseudo-octahedral Ni(II) ions bound to *five* or *six* (N,O) donors at an average Ni−ligand distance of 2.06 Å.[7] Magnetic susceptibility experiments have indicated that, in the *jack bean* urease, the high-spin nickel(II) ions ($S = 1$) are

[†] Universidad de Oviedo.
[‡] The Pennsylvania State University.
[§] Current address: Laboratoire de Dynamique Moleculaire. Institut Jean-Pierre Ebel, 41 rue Jules Horowitz, 38027 Grenoble (France).

(1) Karplus, P. A.; Pearson, M. A.; Hausinger, R. P. *Acc. Chem. Res.* **1997**, *30*, 330−337.
(2) Wolfenden, R.; Snider, M. J. *Acc. Chem. Res.* **2001**, *34*, 938−945.
(3) Covacci, A.; Telford, J. L.; Del Giudice, G.; Parsonnet, J.; Rappuoli, R. *Science* **1999**, *284*, 1328−1333.
(4) Ha, N.-C.; Oh, S.-T.; Sung, J. Y.; Cha, K. A.; Lee, M. H.; Oh, B.-H. *Nat. Struct. Biol.* **2001**, *8*, 505−509.
(5) Thauer, R. K. *Science* **2001**, *293*.
(6) Ciurli, S.; Benini, S.; Rypniewski, W. R.; Wilson, K. S.; Miletti, S.; Mangani, S. *Coord. Chem. Rev.* **1999**, *190−192*, 331−355.
(7) Wang, S.; Lee, M. H.; Hausinger, R. P.; Clark, P. A.; Wilcox, D. E.; Scott, R. A. *Inorg. Chem.* **1994**, *33*, 1589−1593.

10.1021/ja030145g CCC: $25.00

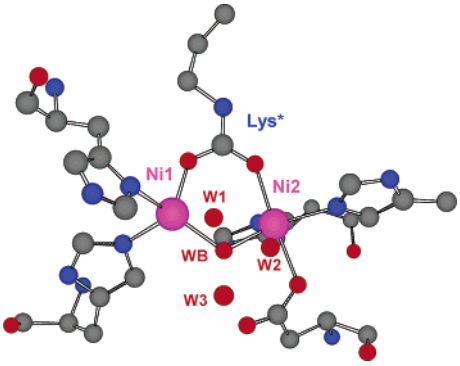

Figure 1. Active site of the dinickel urease enzyme from *K. aerogenes* as determined by X-ray crystallography (PDB Code 1FWJ).

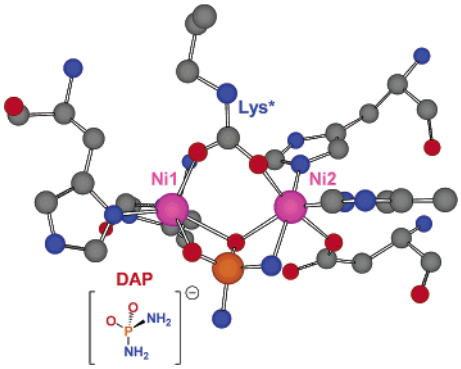

Figure 2. Active site of the dinickel urease enzyme from *B. pasteurii* inhibited by DAP as determined by X-ray crystallography (PDB Code 3UBP).

octahedrally coordinated and have a weak antiferromagnetic coupling characterized by a *J* coupling constant of only −6.3 cm^{-1}.[8] In 1995, the crystal structure at 2.2 Å of urease from *Klebsiella aerogenes* was reported (PDB code: 1KAU).[9] This X-ray structure revealed the presence of two nickel ions 3.5 Å apart, but with *four*- and *five*-coordination. The structural discrepancy between the X-ray and XAS data was later resolved when a new model for the native *K. aerogenes* enzyme (PDB code: 1FWJ) and the crystal structure of the urease from *Bacillus pasteurii* (PDB code: 2UBP) were reported.[10] In these structures, the active site resembles a dinuclear complex in which a distorted squared-pyramidal (Ni1) and an octahedral (Ni2) geometry are interconnected via two shared ligands: one water molecule (WB) and a carbamylated lysine. The presence of this carbamylated lysine explains why CO_2 is required for the ureases to be active.[1] In addition, the Ni1 ion is coordinated by imidazole groups from two different histidine residues and a water molecule (W1) while Ni2 is also coordinated by two histidines, the side chain of an Asp group, and one water molecule (W2) (see Figure 1).

In the ureases, the position of the active site water molecules is important.[6,10] A fourth water molecule (W3) strongly interacts with the bridging water molecule WB, W1, and W2 through short hydrogen bonds. Furthermore, W1 and W2 also establish van der Waals contacts with other conserved residues positioned in order to act as hydrogen bond donors in the vicinity of Ni1 and as hydrogen bond acceptors in the vicinity of Ni2. For example, W1 is ∼3 Å from a protonated Nϵ@His219 atom (*K. aerogenes* numbering) while W2 forms a strong hydrogen bond with the mainchain carbonyl group of Ala167. These contacts are thought to be important for both substrate binding and catalysis.

The structure of the apo-urease from *K. aerogenes* in which the Ni ions were chemically removed has been also determined.[11] In this structure, the bridging lysine residue is not carbamylated. Interestingly, the Cα atoms in this structure have a very small root-mean-squared deviation with respect to those in the nickel-containing enzyme indicating that the architecture of the urease is well adapted to bind the nickel ions without having to undergo large conformational rearrangements. Similarly, other crystallographic studies of urease mutants revealed again the conformational rigidity of the nickel-coordinating residues.[12] In contrast, a helix-turn-helix flap of residues lining the active site cavity has been shown crystallogaphically to be quite flexible: this flap has been observed in an "open" or "closed" conformation for the *K aerogenes* or *B. pasteurii* enzymes, respectively.[6] Changes in the flap conformation, besides controlling the accessibility of the active site, could be important for catalysis.

The crystal structures of the *B. pasteurii* urease complexed with a thiol inhibitor (β-ME) and a diamidophosphate (DAP) compound have provided further insight into the inhibition and catalytic mechanism of the ureases.[6] Most interestingly, in the DAP inhibited enzyme (PDB code 3UBP), it was unambiguously determined that DAP was bound to Ni1 and Ni2 through one O and one N atom, respectively, while the second DAP O atom bridges the metal ions (see Figure 2). This mode of binding has been proposed to mimic a transition state analogue in which urea would act as a chelating agent and the bridging hydroxide would act as the nucleophile.[6]

Proposed Reaction Mechanisms. Based on the available X-ray structures as well as on biochemical and mutagenesis studies, two reaction mechanisms[10,13] have been proposed which mainly differ in the identity of the acid/base catalyst and the protonation state of the nearby His320 residue (see Figure 3). Both mechanisms assume that urea would bind in a bidentate manner displacing W1−W3 as suggested by the crystal structure of the DAP-inhibited urease. The urea carbonyl group would bind to the most electrophilic Ni1 site while one amino end of urea would coordinate to Ni2. This mode of binding is thought to reduce the resonance stabilization of urea facilitating the ability of the bridging hydroxide to attack the carbonyl carbon atom to give a tetrahedral intermediate. According to the proposal by Benini et al.,[10] the bridging hydroxide group can also act as the general acid donating its H atom to the leaving ammonia molecule which, in turn, would interact with His320. These authors also speculate that proton transfer could be assisted by the carboxylate group ligated to Ni2. Alternatively, Karplus et al. suggest that protonation occurs via the general acid His320 (i.e., His320 is protonated in the native form of the enzyme).[1,13] However, these authors do not entirely rule out that a metal bound water molecule (W2) would act as the

(8) Clark, P. A.; Wilcox, D. E. *Inorg. Chem.* **1989**, *28*, 1326−1333.
(9) Jabri, E.; Carr, M. B.; Hausinger, R. P.; Karplus, P. A. *Science* **1995**, *268*, 998−1004.
(10) Benini, S.; Rypniewski, W. R.; Wilson, K. S.; Miletti, S.; Ciurli, S.; Mangani, S. *Structure* **1999**, *7*, 205−216.
(11) Pearson, M. A.; Schaller, R. A.; Michel, L. O.; Karplus, P. A.; Hausinger, R. P. *Biochemistry* **1998**, *37*, 6214−6220.
(12) Jabri, E.; Karplus, P. A. *Biochemistry* **1996**, *35*, 10616−10626.
(13) Pearson, M. A.; Park, I.-L.; Schaller, R. A.; Michel, L. O.; Karplus, P. A.; Hausinger, R. P. *Biochemistry* **2000**, *39*, 8575−8584.

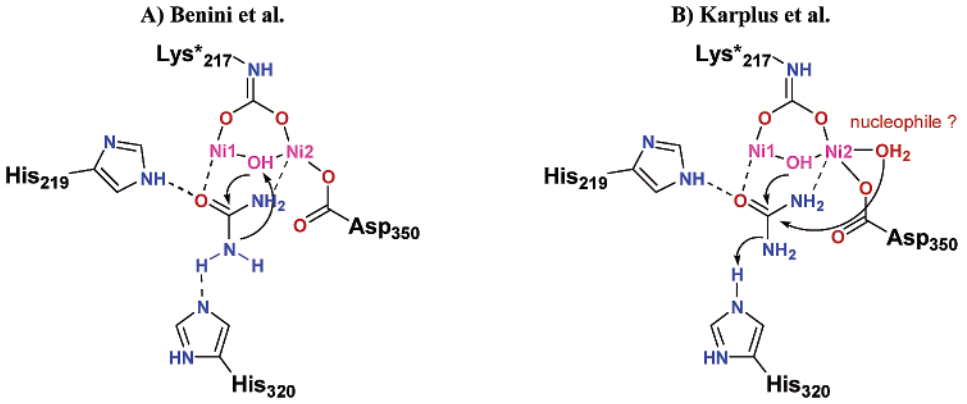

Figure 3. Proposed reaction mechanisms based on X-ray, kinetic, and mutagenesis data.

nucleophile. To support their mechanistic proposals, Karplus et al. argue that the pH dependence of wild-type urease is consistent with a reversed protonation mechanism in which an activated Ni2-bound water molecule or the bridging oxo-dianion of WB ($pK_a \approx 9$) acts with the general acid His320 ($pK_a \approx 6.5$) to achieve catalysis.

Considerable effort has been also devoted to the search of model complexes featuring a dinickel core bound to urea in order to mimic the enzymatic reactivity of ureases. [14−18] In a few cases, the urease-like models exhibit reactivity pertinent to the ureases. For example, it has been reported that urea at a model dinickel center undergoes ethanolysis[19] while other complexes promote the elimination of ammonia at high temperatures from a coordinated urea.[20] Another model complex has been shown to be able to decompose urea into ammonia and cyanic acid 500 times faster than the observed process in aqueous solution, suggesting an alternative mechanism for the urease-catalyzed hydrolysis of urea via a cyanate intermediate.[21]

Goals for the Present Work. Although X-ray studies of the ureases have provided data regarding the structure of these enzymes, many fundamental questions about the environment of the nickel ions and the mode of urea binding remain poorly understood at the molecular level. Several theoretical studies on urease have been reported in the literature. Zimmer et al. have used molecular mechanics methods to study substrate and inhibitor binding to urease,[22,23] while Musiani et al. have used the Dock program to dock substrate and inhibitors into the urease active site.[24] From these studies, these authors have made qualitative arguments regarding the mechanism of urease. In general, however, classical models are not as effective as quantum chemical approaches in understanding metal containing systems, so the studies reported to date are qualitative in nature. In this article, we report a computational study of the electronic structure of cluster models representing the nickel centers of urease that gives insight into the nature of the contacts between the nickel ligands, the strength and flexibility of the Ni1−WB−Ni2 bridge, the location of the mechanistically relevant water molecules, the protonation state of the dinickel complex, the relative stability of the monodentate versus bidentate modes of urea binding, and so forth. By using the formalism of density functional theory, we also estimate the exchange coupling parameters for the models of the native active site of ureases. Finally, we explore two reaction mechanisms for the hydrolysis of urea starting from monodentate and bidentate urea-bound complexes, respectively. Following the available mechanistic proposals, we have studied both possibilities that the Ni1···Ni2 bridging hydroxide or the Ni2-bound water are the hydrolytic water molecules. Moreover, the geometries and relative energies of the transition structures and intermediates will be helpful in increasing our understanding of the origin of the catalytic efficiency of the ureases.

Methods

The computational study of open-shell transition metal complexes can be efficiently carried out using the density functional theory (DFT) methods[25] implemented in Jaguar v3.5−v4.1[26] and Gaussian 98.[27] In particular, the dinuclear systems studied herein were subjected to energy minimizations using the B3LYP functional[28] with the double-ζ 6-31G* basis set[29] for nonmetal atoms and the Los Alamos effective core potentials[30−32] for the metal atoms (this mixed basis set will be denoted as LACVP*). The use of effective core potentials for Ni ions was calibrated by comparing the geometries, energies, and charges for a series of Ni−L complexes (L = OH^-, H_2O, CH_3COO^-, etc.) by using the LACVP*, 6-31G*, and 6-311G** basis sets for Ni. All the test calculations are presented in the Supporting Information.

(14) Wages, H. E.; Taft, K. L.; Lippard, S. J. *Inorg. Chem.* **1993**, *32*, 2, 4985−4987.
(15) Koga, T.; Furutachi, H.; Nakamura, T.; Fukita, N.; Ohba, M.; Takahashi, K.; Okawa, H. *Inorg. Chem.* **1998**, *37*, 989−996.
(16) Meyer, F.; Pritzkow, H. *J. Chem. Soc., Chem. Commun.* **1998**, 1555−1556.
(17) Barrios, A. M.; Lippard, S. J. *J. Am. Chem. Soc.* **1999**, *121*, 11751−11757.
(18) Carlsson, H.; Haukka, M.; Nordlander, E. *Inorg. Chem.* **2002**, *41*, 4981−4983.
(19) Yamaguchi, K.; Koshino, S.; Akagi, F.; Suzuki, M.; Uehara, A.; Suzuki, S. *J. Am. Chem. Soc.* **1997**, *119*, 5752−5753.
(20) Meyer, F.; Kaifer, E.; Kircher, P.; Heinze, K.; Pritzkow, H. *Chem.—Eur. J.* **1999**, *5*, 1617−1630.
(21) Barrios, A. M.; Lippard, S. J. *J. Am. Chem. Soc.* **2000**, *122*, 9172−9177.
(22) Zimmer, M. *J. Biomol. Struct. Dyn.* **2000**, *17*, 787−797.
(23) Csiki, C.; Zimmer, M. *J. Biomol. Struct. Dyn.* **1999**, *17*, 121−131.
(24) Musiani, F.; Arnofi, E.; Casadio, R.; Ciurli, S. *J. Biol. Inorg. Chem.* **2001**, *6*, 300−314.
(25) Koch, W.; Holthausen, M. C. *A Chemist's Guide to Density Functional Theory*, 2nd ed.; Wiley-VCH: New York, 2001.
(26) *Jaguar*, 3.5 ed.; Schrödinger, Inc.: Portland, OR, 1998.
(27) Frisch, M. J.; Trucks, G. W.; Schlegel, H. B.; Scuseria, G. E.; Robb, M. A.; Cheeseman, J. R.; Zakrzewski, V. G.; Montgomery, J. A.; Stratmann, J., R. E.; Burant, J. C.; Dapprich, S.; Millam, J. M.; Daniels, A. D.; Kudin, K. N.; Strain, M. C.; Farkas, O.; Tomasi, J.; Barone, V.; Cossi, M.; Cammi, R.; Mennucci, B.; Pomelli, C.; Adamo, C.; Clifford, S.; Ochterski, J.; Petersson, G. A.; Ayala, P. Y.; Cui, Q.; Morokuma, K.; Malick, D. K.; Rabuck, A. D.; Raghavachari, K.; Foresman, J. B.; Cioslowski, J.; Ortiz, J. V.; Stefanov, B. B.; Liu, G.; Liashenko, A.; Piskorz, P.; Komaromi, I.; Gomperts, R.; Martin, R. L.; Fox, D. J.; Keith, T.; Al-Laham, M. A.; Peng, C. Y.; Nanayakkara, A.; Gonzalez, C.; Challacombe, M.; Gill, P. M. W.; Johnson, B.; Chen, W.; Wong, M. W.; Andres, J. L.; Gonzalez, C.; Head-Gordon, M.; Replogle, E. S.; Pople, J. A. *Gaussian 98*, A.6 ed.: Pittsburgh, PA, 1998.
(28) Becke, A. D. In *Modern Electronic Structure Theory Part II*; Yarkony, D. R., Ed.; World Scientific: Singapore, 1995.
(29) Hehre, W. J.; Radom, L.; Schleyer, P. v. R.; Pople, J. A. *Ab Initio Molecular Orbital Theory*; John Wiley & Sons: New York, 1986.
(30) Hay, P. J.; Wadt, W. R. *J. Chem. Phys.* **1985**, *82*, 270−283.
(31) Hay, P. J.; Wadt, W. R. *J. Chem. Phys.* **1985**, *82*, 299−310.
(32) Wadt, W. R.; Hay, P. J. *J. Chem. Phys.* **1985**, *82*, 284−298.

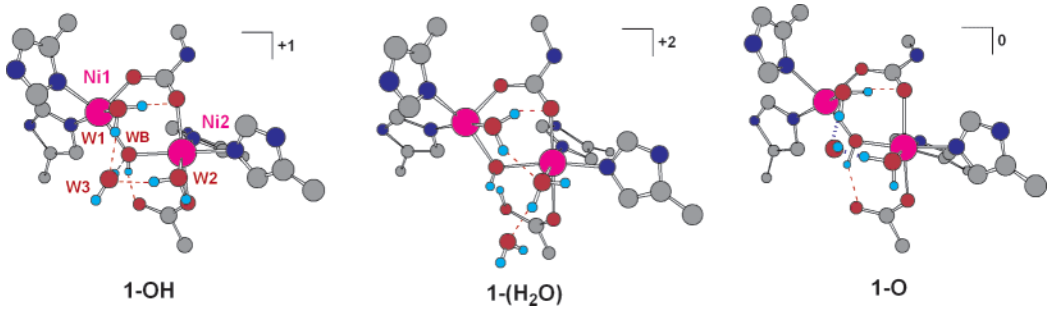

Figure 4. B3LYP/LACVP* optimized structures of the **1-OH**, **1-H_2O**, and **1-O** dinickel complexes. For the sake of clarity, some H atoms are not represented in the ball-and-stick models.

Each nickel ion contained in the dinickel model complexes contains two electrons which have parallel unpaired spins (high-spin case). To handle this aspect of the urease system, we used the *restricted* open-shell implementation of the B3LYP density functional available in Jaguar in order to explore the potential energy surface (PES) of the dinickel complexes in their high-spin state (a quintet state). The use of an automated SCF guess methodology was required in order to achieve convergence of the quintet wave function to the ground electronic state.[33]

Geometry optimizations of the large dinickel systems at the B3LYP/LACVP* level of theory used a Broyden−Fletcher−Goldfarb−Shanno (BFGS) minimizer until the maximum force and the root-mean-squared (RMS) force were below 0.001 00 and 0.000 30 au, respectively. To locate transition structures on the PES, we employed the synchronous transit quasi-Newton method STQN implemented in Jaguar. To characterize the critical points located on the B3LYP/LACVP* PES, we carried out numerical frequency calculations (unfortunately, analytical frequencies at the ROB3LYP/LACVP* level were not available in Jaguar). However, the large size of the dinickel systems (76−79 atoms) prevented us from carrying out full numerical frequency calculations. Hence, we decided to carry out partial and numerical Hessian calculations for selected atoms including the W1−W3 molecules and/or the urea fragment in the optimized structures modeling the water- and urea-bound forms of the dinickel active site. For the critical points modeling the hydrolysis of the urea molecule, the corresponding subsystems for the numerical frequency calculations were augmented by including other reactive atoms (e.g., WB and the Ni2-bound carboxylate group). Of course, this computational approach is a compromise between cost and accuracy. Globally, the partial and numerical frequency calculations allowed us to qualitatively characterize the corresponding critical points as minima or transition structures depending on the presence of zero or one imaginary frequency, respectively. Moreover, in the case of the imaginary frequencies, animation of their transition vectors further confirmed the nature of the reactive processes.

After geometry optimization, the electronic energies of the dinickel complexes were refined by means of single-point calculations using the 6-311+G(2d,2p) basis set for nonmetal atoms and a modified version of the LACVP core potentials for Ni in which the exponents were decontracted to form a triple-ζ quality basis set (this basis set is denoted as LACV3P**+).[34] Atomic charges were computed by carrying out natural population analysis[35] (NPA) using the B3LYP/LACV3P**+ density matrices.

To obtain a gross estimation of the influence of the environment polarity on the relative energies, we computed the solvation energies of the dinickel complexes by means of single-point B3LYP/LACVP* PB-SCRF (Poisson−Boltzmann self-consistent reaction field) calculations, where the solute is represented by a set of atomic charges, and the solvent (water) is represented as a layer of charges at the solvent-exposed molecular surface.[36]

Since the two nickel ions in the active site of ureases are only weakly antiferromagnetically coupled, the quintet PES studied at the B3LYP/LACVP* level, which formally corresponds to a ferromagnetic state, can provide accurate energetic and geometric data. However, we also estimated the exchange coupling parameter (J) for several model complexes within the context of the Heisenberg spin operator formalism. We modeled the spin manifold as proposed by Zhao et al.[37] and extracted a J value from the splitting between the ferromagnetic (F, high spin) and antiferromagnetic (AF) states. The AF state, whose representation by DFT calculations is only approximate, is represented by a *broken* symmetry (BS) or low-spin state in which the spin on the two nickel ions are antiparallel. The F state was converged by means of a single-point unrestricted UB3LYP calculation using the LACV3P**+ basis set on the B3LYP optimized structures. The BS wave function was obtained using the computational procedure proposed by Dunietz et al.:[34] (1) an F state was converged, (2) the resultant DFT orbitals were localized according to the Boys localization scheme, and (3) an initial guess for the BS state was then constructed from the localized orbitals, by assigning paired spins to the corresponding localized orbitals on each nickel atom. In all the analyzed structures, the converged AF state showed nearly complete spin localization on the nickel centers.

Results and Discussion

Dinickel Complexes Modeling the Active Site of Ureases. Initially, we considered several cluster models which differed in the protonation state of the bridging water molecule (i.e., WB = OH^-, H_2O, O^{2-}). In these models, the nickel(II) ions were complexed by four methyl-imidazole ligands, the carboxylate of the Asp side chain, and the carbamylate group of Lys*. The important water molecules W1 and W2 were coordinated to Ni1 and Ni2, respectively, and the free active site water (W3) was included in the cluster models. The initial geometries were built by molecular modeling from the X-ray coordinates of the urease from *K. aerogenes* (PDB ID code: 1FWJ). To prevent movement of groups of atoms to locations unattainable in the actual ureases, the Cβ atoms (methyl groups except the one attached to the carbamylate group) were held in the relative position found in the 1FWJ crystal structure throughout the computations. We note, however, that the resultant models were still reasonably flexible.

Figure 4 shows the optimized structures of the dinickel complexes representing the active site of the native urease

(33) Vacek, G.; Perry, J. K.; Langlois, J.-M. *Chem. Phys. Lett.* **1999**, *310*, 189.
(34) Dunietz, B. D.; Beachy, M. D.; Cao, Y.; Whittington, D. A.; Lippard, S. J.; Friesner, R. A. *J. Am. Chem. Soc.* **2000**, *122*, 2828−2839.
(35) Reed, A. E.; Weinstock, R. B.; Weinhold, F. *J. Chem. Phys.* **1985**, *83*, 735−746.
(36) Tannor, D. J.; Marten, B.; Murphy, R.; Friesner, R. A.; Sitkoff, D.; Nicholls, A.; Ringnalda, M.; Goddard, I., W. A.; Honig, B. *J. Am. Chem. Soc.* **1994**, *116*, 11875−11882.
(37) Zhao, X. G.; Richardson, W. H.; Chen, J.-L.; Li, J.; Noodleman, L. *Inorg. Chem.* **1997**, *36*, 1198−1217.

Table 1. B3LYP/LACVP* Interatomic Distances in Angstroms for the Series of Dinickel Clusters Representing the Native Form of the Urease Active Site

	Ni1··Ni2	Ni1–WB	Ni2–WB	Ni1–W1	Ni2–W2	Ni1–$O_{\epsilon 1}$	Ni2–$O_{\epsilon 2}$	Ni2–$O_{\delta 1}$	W1–W3	W2–W3	WB–W3	WB–$O_{\delta 2}$
X-ray (1FWJ)	3.59	2.15	1.98	2.09	2.13	2.08	2.08	2.18	2.57	2.38	2.68	2.70
X-ray (2UBP)	3.70	2.11	2.18	2.18	2.21	2.08	2.10	2.21	2.16	2.24	2.26	2.51
1-OH	3.557	1.991	2.071	2.124	2.207	2.009	2.156	2.082	2.747	2.704	2.541	2.650
2-OH	3.748	2.075	2.014	2.181	2.137	2.144	3.475	2.011	2.637	2.641	2.532	2.655
1-(H_2O)	3.565	2.081	2.108	2.143	2.200	2.013	2.107	2.238	2.766 **(W1−W2)**	2.618	3.211	2.516
1-O	3.515	1.942	1.992	2.038	2.065	2.044	2.240	2.106	2.462	2.432	3.415	2.717

enzymes, while Table 1 contains the most important equilibrium distances. Unless otherwise noted, all the relative energies given in the text correspond to the B3LYP/LACV3P**+//B3LYP/LACVP* level of theory (restricted SCF calculations).

For comparative purposes, Table 1 also contains experimental data from the X-ray structures of the native form of urease (1FWJ and 2UBP PDB ID codes). In general, both the Ni1···Ni2 or Ni−ligand distances are quite similar in the computational and experimental structures (see below). We also carried statistical analyses on selected Ni−ligand distances in the X-ray structures available in the Cambridge Structural Database (CSD). For example, the average Ni−O(bridging hydroxide), Ni−O(monodentate carboxylate), and Ni−O(water) distances in the CSD database are 2.06 ± 0.07 Å, 2.05 ± 0.06 Å, and 2.08 ± 0.05 Å, respectively, in reasonable agreement with the analogous bond distances in our computational models.

A. WB → OH^-. The **1-OH** model, in which the bridging WB molecule is a hydroxide anion, resembles the experimentally observed coordination mode of the nickel ions in the ureases. The root-mean-squared deviation (RMSD) between the 1FWJ X-ray structure and **1-OH** is 0.44 Å (the RMSD values were computed between heavy atoms in the side chains coordinated to the nickel ions and in the Ni1−WB−Ni2 bridge while those of W1−W3 were omitted). Moreover, the computed Ni1···Ni2 distance (3.56 Å) is in good agreement with the X-ray data (3.59 Å in the 1FWJ model; see also other distances in Table 1). In **1-OH**, the Ni2 ion has a nearly perfect octahedral coordination (e.g., the average W2−Ni2−X angle with the equatorial donor atoms around Ni2 is 88°), while Ni1 shows a slightly distorted square-pyramidal coordination with the Oϵ1@Lys* atom being in the apical position (the average Oϵ1−Ni1−X angle is 100°). The sequence of hydrogen bonds and the positioning of the W1−W3 molecules were comparable with the topology of the crystallographic water molecules. Thus, W3 bridges the W1 and W2 water molecules and simultaneously forms a short hydrogen bond with WB, which, in turn, is hydrogen bonded with the carboxylate group coordinated to Ni2 (see Figure 4). W1 also gives a hydrogen bond with the Oϵ2 atom of the bridging carbamylate, although this contact could be substantially weakened upon inclusion of environmental effects. The equilibrium distances between heavy atoms involved in the hydrogen bonds (O···O 2.6−2.7Å; typical of O···HO interactions) are larger than those observed in the X-ray data (2.0−2.2Å) (the unusually short X-ray distances suggest that these waters are quite mobile in the solid state). Overall, we conclude that the **1-OH** cluster accurately models the native form of the urease active site.

B. WB → H_2O. In the optimized **1-(H_2O)** model, the WB molecule was initially neutral. However, during geometry optimization, WB donated one of its protons to the Oδ2 atom of the Asp carboxylate group to give a hydroxide bridge, Ni1−OH−Ni2. This is in agreement with the calculations on the small Ni-L complexes: a neutral carboxylic is a better nickel ligand than a simple H_2O molecule, while a hydroxide anion is a better ligand than a carboxylate (see Supporting Information). The nickel ions in **1-(H_2O)** are bridged by the hydroxide and the carbamylate group as in **1-OH**, resulting in an Ni1···Ni2 separation of 3.57 Å. Despite the different global charge of **1-(H_2O)** (+2) with respect to that of **1-OH** (+1), the coordination spheres around Ni1 and Ni2 were a distorted square-pyramid and an octahedron, respectively, and the Ni1···Ni2 separation was nearly identical in both structures. The RMSD value of **1-(H_2O)** with respect to the equivalent heavy atoms in the 1FWJ structure (0.45 Å) basically coincides with that computed for **1-OH**. Thus, **1-(H_2O)** is equally compatible with the main structural features of the nickel ions in the urease active site. Some geometric differences between **1-OH** and **1-(H_2O)** arise in the sequence of hydrogen bonds interconnecting the W1−W3 molecules with WB: in **1-(H_2O)**, W1 and W2 establish a direct hydrogen bond contact, while W3 interacts only with W2.

C. WB → O^{2-}. Importantly, we found that the oxo-dianion bridge is not stable in the dinickel cluster models. During energy minimization, the original O^{2-} at the WB position captured a proton from the W3 molecule, which then becomes a hydroxide anion tightly bound to W1 and W2. This observation suggests that deprotonating a water molecule would be more likely than deprotonating the hydroxide moiety in the Ni1−OH−Ni2 bridge in the native structure of the enzyme. Inspection of the optimized **1-O** model reveals its similarity with the **1-OH** model: the Ni1···Ni2 separation is 3.52 Å, the Ni1 and Ni2 ions exhibit five- (squared-pyramidal) and six-coordination (octahedral), and the topologies of the hydrogen bonds involving the W1−W3 and WB molecules were also similar. The RMSD of **1-O** with respect to the X-ray data is 0.43 Å.

The fact that the Ni1−(O^{2-})−Ni2 bridge is unstable in the cluster models of the ureases can be interpreted in terms of the coordination geometry of the nickel(II) ions in the enzyme. The positioning of the nickel ligands forces the Ni1−WB−Ni2 bridge into a nonlinear geometry (e.g., the Ni1−O−Ni2 angles in **1-OH** and **1-(H_2O)** are 122° and 117°, respectively), while the oxo-bridge prefers a linear arrangement. Altogether, our theoretical data allow us to safely discard the oxo-dianion bridge between the nickel ions in the native form of the ureases. Of course, this is in agreement with the weak magnetic Ni1···Ni2 coupling observed experimentally (see below).

Flexibility of the Ni1−OH−Ni2 Bridge. In **1-OH**, **1-(H_2O)**, and **1-O**, the nickel ions share the WB hydroxide and the

Scheme 2

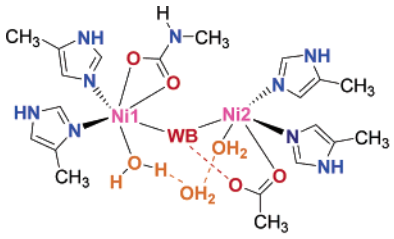

2

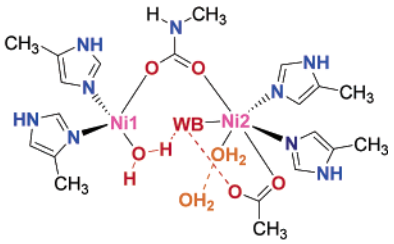

3

carbamylate group. However, other possible arrangements could be potentially accessible through a *flexible* Ni1···Ni2 interaction. We considered several hypothetical structures involving the loss of the carbamylate bridge (**2**) or the hydroxide bridge (**3**), as shown in Scheme 2. We investigated the stability of these configurations at the B3LYP/LACVP* level assuming a global charge of either +1 (i.e, unprotonated Asp) or +2 (protonated Asp).

We carried out four different geometry optimizations which we labeled as **2-OH**, **3-OH**, **2-H_2O**, and **3-H_2O**. We found that only **2-OH** is a stable energy minimum on the B3LYP/LACPV* PES. The rest of the initial configurations (**2-H_2O**, **3-OH**, **3-H_2O**) converged on the doubly bridged structures **1-OH** and **1-(H_2O)**. This computational observation is indicative of a *rigid* Ni1···Ni2 structural feature in the model complexes of the active site of ureases, especially in the case of the **1-(H_2O)** structure with a global charge of +2.

In the optimized model **2-OH** (Figure S2 in the Supporting Information), the carbamylate group binds to Ni1 in a symmetric bidentate manner. The coordination of Ni1 is well described as a distorted octahedral environment in which the carbamylate group, the W1 molecule, and one imidazole ring lie in the equatorial plane. The loss of the carbamylate bridge has only a moderate impact on the Ni1···Ni2 separation which is now 3.75 Å (3.56 Å in **1-OH**). The Ni2 ion is surrounded by a squared-pyramidal coordination polyhedron with the Oδ1@Asp atom occupying the axial position. In fact the location of the Ni2 ligands hardly changes with respect to that in the **1-OH** structure. As expected, **2-OH** is less stable than the doubly bridged structure **1-OH**. The computed energy difference (9.7 kcal/mol) is moderate.

Estimation of Exchange Coupling Parameters. The broken symmetry (BS) and ferromagnetic (F) states of the dinickel complexes were modeled by means of open-shell B3LYP wave functions as described in the Methods section. In the Heisenberg formalism and the broken symmetry approach, the coupling parameter J can be calculated using the following equation:[37]

$$J = -(E_F - E_{BS})/(4S_1S_2)$$

where S_1 and S_2 are the spin quantum numbers (+1) for each nickel ion. This equation also assumes that both nickel ions are equivalent in the dinuclear complex. Table 2 presents splitting energies ($E_F - E_{BS}$) calculated for the small dinuclear complexes Ni−X−Ni (X = O^{2-}, OH^-) and the large cluster models **1-OH**, **1-(H_2O)**, and **1-O**.

For the oxo-bridged $[Ni-O-Ni]^{2+}$ complex, the F state is 3.4 kcal/mol above the BS state, resulting in an estimated J value of about −300 cm^{-1}. For the hydroxide-bridged $[Ni-OH-Ni]^{3+}$complex, the F state (high spin) is slightly more stable than the BS (low spin) by only 0.1 kcal/mol which results in a very small positive J value of ∼9 cm^{-1}. Thus, our calculations indicate that the linear oxo-bridged compound would exhibit a strong antiferromagnetic coupling in agreement with its electronic structure (i.e., short Ni−O distances with large charge delocalization) and in agreement with previous theoretical work using a multireference approach.[38] In contrast, the hydroxide-bridged complex, which has more ionic character, has only a small magnetic coupling.

Table 2. Splitting Energy of the Different Dinickel Complexes

structure	spin state energy[a] (au) BS (broken symmetry)	spin state energy[a] (au) F (high spin)	energy splitting (kcal/mol)
[Ni−O−Ni]$^{2+}$	−413.0605	−413.0550	3.4
[Ni−OH−Ni]$^{3+}$	−412.9896	−412.9897	−0.1
1-OH	−2218.9640	−2218.9642	−0.1
1-H_2O	−2219.2982	−2219.2981	0.1
1-O	−2218.4822	−2218.4818	0.2

[a] From UB3LYP/LACVP**+ calculations on the B3LYP/LACVP* geometries.

The calculated splitting between the high-spin and broken symmetry states for the large dinuclear complexes modeling the active site of ureases are quite small, ±0.1 kcal/mol. This was not entirely unexpected since the three complexes **1-OH**, **1-(H_2O)**, and **1-O** all have the Ni1−OH−Ni2 bridge. In terms of J values, our calculations predict that the Ni ions in **1-OH** would be weakly ferromagnetically coupled (J = +9 cm^{-1}), whereas both **1-(H_2O)** and **1-O** would be weakly antiferromagnetic (J = −10, −20 cm^{-1}). However, in view of the uncertainties in the DFT methodology, the broken symmetry approach, the accuracy of the SCF calculations, and so forth, we note that *all* the dinuclear complexes are consistent with the experimental observation of weak antiferromagnetic coupling in the active site of ureases, as long as the calculated splitting energies are very small. We also note that the additional energy stabilization due to magnetic coupling would be almost negligible.

Binding of Urea. Since urea is a relatively small molecule, QM calculations on cluster models can give significant insights into the most relevant binding orientations. As discussed above, the mechanistic proposals favor a bidentate mode of binding for urea. In this model, urea binds to Ni1 through its carbonyl group while one amino end is coordinated to Ni2. However, monodentate adducts in which the carbonyl group of urea is coordinated to Ni1 and the Ni2-bound W2 molecule is present (or absent) are also interesting possibilities. In addition, the results obtained for the dinickel complexes representing the

(38) Wang, C.; Fink, K.; Staemmler, V. *Chem. Phys. Lett.* **1995**, *192*, 25−35.

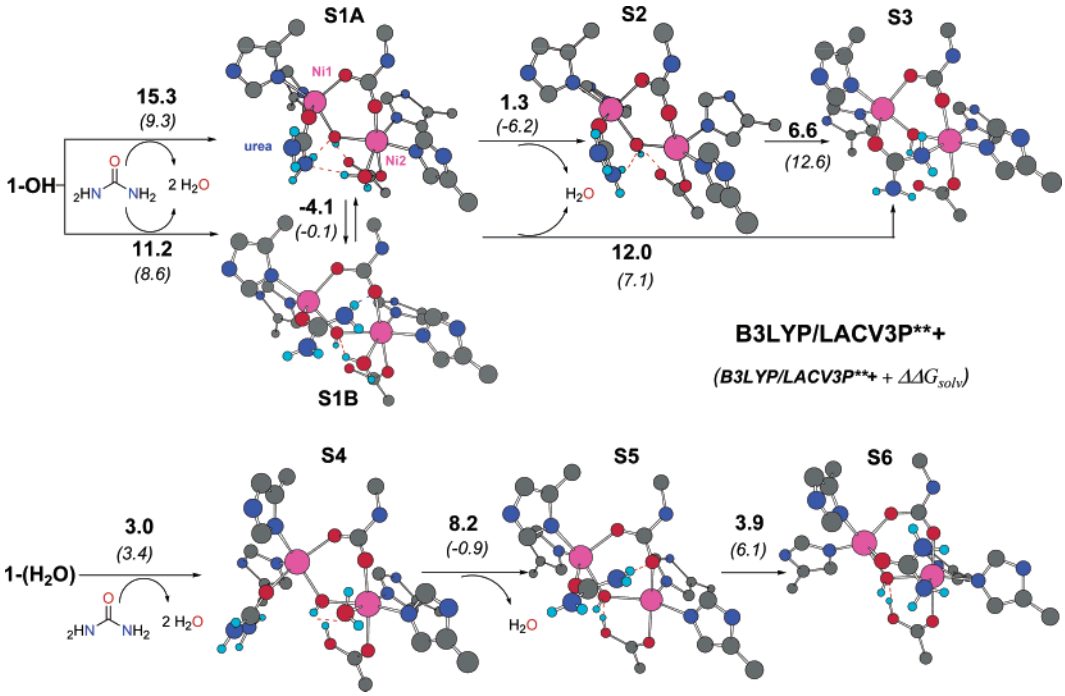

Figure 5. B3LYP/LACVP* optimized structures of the urea-bound complexes. B3LYP/LACV3P**+ //B3LYP/LACVP* reaction energies (in bold type) in the gas phase are given in kcal/mol. Reaction energies in water solution are also indicated between parentheses. For the sake of clarity, some H atoms are not represented in the ball-and-stick models.

unbound form of the ureases (**1-OH** and **1-(H_2O)**) indicate that two protonation states (i.e., protonated and unprotonated carboxylate) should be considered in the urea-bound complexes. Based on these considerations, we characterized a series of dinickel complexes in the presence of urea as models for the preferred urea-binding mode of the ureases.

To examine the monodentate urea-bound dinickel clusters, the starting geometries were obtained by replacing the W1 and W3 molecules by the carbonyl group of urea and one amino group, respectively, in structures **1-OH** and **1-(H_2O)**. For the bidentate urea-bound complexes, W2 was removed, and an sp^3 hybridized urea amino group was bound to Ni2. Two different orientations of the free amino end of urea were considered. Some of these initial structures with a bidentate mode of urea binding were not stable on the B3LYP/LACVP* PES and evolved into monodentate adducts during energy minimization (see below).

We first describe the optimized complexes that were derived from the **1-OH** cluster model (structures **S1A**, **S1B**, **S2**, and **S3** shown in Figure 5; some important equilibrium distances are collected in Table S2 in the Supporting Information). The structure of **S1A** shows that binding of urea is compatible with the presence of the W2 molecule. After having displaced W1 and W3, urea binds to Ni1 through its carbonyl group (O···Ni1 = 2.139 Å) while one amino end of urea has a H-bond contact with the bridging hydroxide (N···O(WB) = 2.672 Å). The remaining W2 molecule also contributes to the binding of urea by establishing a hydrogen bond with one amino end (O···N = 2.904 Å). The positions of the rest of the nickel ligands are unaltered upon urea binding, while the Ni1···Ni2 distance (3.510 Å) is slightly lower than that in **1-OH**. The monodentate urea-bound complex **S1B** is quite similar to **S1A**, although both complexes differ in the presence or absence of H-bonds. In **S1B**, urea interacts with the nickel-bridging carbamylate group (N(urea)···O = 2.806 Å) while the W2 molecule acts as a proton donor to give a short hydrogen bond with WB (O(W2)··· O(WB)) = 2.594 Å). The strength of the W2··· WB interaction explains why **S1B** is 4.1 kcal/mol more stable than **S1A**. Most interestingly, the W2 molecule in **S1B** lies in a nearly perpendicular position with respect to urea, which is appropriate for nucleophilic attack toward the carbonyl C atom of urea with concomitant proton abstraction by WB. The C(urea)···O(W2) separation is only 3.061 Å in **S1B** (3.561 Å in **S1A**), confirming that **S1B** is a *prereactive* complex.

In the absence of the W2 molecule, we located **S2** (Figure 5) which has a monodentate urea binding mode. Apart from the presence or absence of W2, the coordination of the nickel ions in the **S1A** and **S2** models is quite similar. The same interactions anchor urea to the Ni ions in both complexes: the carbonyl group of urea is coordinated to Ni1 with a distance of 2.133 Å in **S2**, and one amino group maintains the hydrogen bond contact with WB. Although the WB oxygen is 3.122 Å away from the carbonyl C atom of urea in **S2**, its orientation is not optimal for nucleophilic attack given that WB and urea are nearly coplanar.

In the bidentate adduct **S3** between urea and the dinickel cluster, the urea molecule lies nearly parallel to the Ni1−OH−Ni2 bridge (see Figure 5). The carbonyl group and one amino group of urea bind to Ni1 and Ni2, respectively, with equilibrium distances of 2.252 (Ni1···O) and 2.329 Å (Ni2···N). The change in the mode of urea binding does not substantially alter the coordination environment around the nickel centers with respect to the monodentate complexes. However, the resonance stabilization of urea is clearly disrupted in the bidentate complex **S3**. Thus, both amino groups of urea become slightly pyramidalized in **S3** (the sum of the X−N−Y angles around N1 and N2 is 347° and 344°, respectively), and the C−N1 (1.394 Å) and C−N2 (1.353 Å) bond lengths are dissimilar. Most interestingly, the separation between the oxygen atom in the bridging hydroxide (WB) and the carbonyl C atom in urea is very short, only 2.686 Å. Moreover, the hydroxide group is almost perpendicular to urea. Therefore, **S3** corresponds to a

prereactive complex in which the resonance stabilization of urea is partially lost and the bridging hydroxide is positioned for nucleophilic attack on the carbonyl group.

The energetic changes involved in the urea binding process are also indicated in Figure 5. From **1-OH**, formation of the bidentate adduct **S3** proceeds via either three (**1-OH** → **S1A** → **S2** → **S3**) or two (**1-OH** → **S1B** → **S3**) formal steps. The overall process (**1-OH** → **S3**) is uphill in energy by a ΔE of 23.2 kcal/mol. This value does not include the nickel−urea interactions as a further driving force for urea binding. We note, however, that the global ΔE value is not very large and could be compensated by electrostatic environmental effects, entropic effects (urea acts as a *chelate* ligand), and specific urea−residue contacts in the active site of the ureases. For example, inclusion of electrostatic effects by means of single-point PB-SCRF calculations simulating water stabilizes the bidentate adduct **S3** by 7.5 kcal/mol with respect to **1-OH** + urea (see Figure 5). Other factors (e.g., the dynamics of the active site flap of residues) could also influence the relative stability of the bidentate and monodentate complexes.

S4−**S6** (see Figure 5) are urea-bound complexes with global charges of +2 which arose from the cluster model **1-(H_2O)**. The structure, **S4**, is derived from **1-(H_2O)** with only W2 preserved. Inspection of the equilibrium geometry of **S4** points out that the nickel coordination environments are unaffected by urea binding with respect to **1-(H_2O)**. In **S4**, the unique interaction between urea and the dinickel cluster is the Ni1−carbonyl bond (2.156 Å). On the other hand, the bridging hydroxide (WB) is hydrogen bonded to the Ni2-bound carboxyl (Oδ2···O(WB) = 2.519 Å) and W2 (O(WB)···O(W2) = 2.764 Å). In addition, W2 interacts with the carbamylated lysine through an H-bond contact. In fact, the stability of these H-bond contacts precludes any direct interaction of urea with the important WB−W2 waters in contrast with the **S1A** structure where urea participates in the H-bond network with WB and W2. Thus, the position of urea in **S4** relative to the Ni1−WB−Ni2−W2 moiety is unfavorable for catalysis.

When the three neutral water molecules in **1-(H_2O)** are replaced by urea, two model complexes, **S5** (monodentate) and **S6** (bidentate), were located on the B3LYP/LACVP* PES. Ongoing from the structure **S4** to **S5**, urea reorients in order to interact with the WB molecule and the carbamylate group. Thus, the WB moiety in **S5** acts as a proton donor in a hydrogen bond with the urea carbonyl group (O(WB)···O(urea) = 2.686 Å). Similarly, one amino end of urea forms an N−H···O contact with the Oδ2 atom of the bridging carbamylate with an N····O distance of 2.889 Å. The monodentate structure **S5** can rearrange into the bidentate complex **S6** in which a new bond is formed between the Ni2 center and one amino group of urea (2.364 Å). However, neither **S5** nor **S6** can be considered as prereactive complexes given that the WB hydroxide, which would be the nucleophile, is 3.2−3.5 Å from the carbonyl C atom of urea in an orientation that does not favor nucleophilic attack.

The sequence of steps connecting **1-(H_2O)** with the **S4**−**S6** structures and the corresponding energy changes are indicated in Figure 5. As in the case of the **1-OH** structure, binding of urea to **1-(H_2O)** is an endothermic process with a global energy change ΔE in the gas phase of 15.1 kcal/mol required to yield the bidentate structure **S6** (8.6 kcal/mol in the solvent continuum). Nevertheless, we note again that our energy calculations do not include either entropic contributions or the influence of specific interactions of urea with other residues in the active site of the ureases.

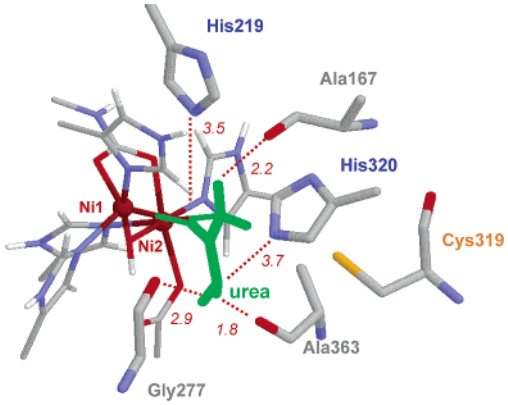

Figure 6. Docked structure of the prereactive complex **S3** within the 1FWJ X-ray structure (*K. aerogenes* residue numbering). Protein atoms were held fixed, and the side chains of the residues liganded to the nickels were replaced by the QM atoms. Some distances are given in Å.

As mentioned above, the cluster models **1-OH** and **1-(H_2O)** were structurally very similar and have very small J values, and therefore, a clear assignment of the best model to represent the native form of ureases was not possible. However, by comparing the structures **S1**−**S3** derived from **1-OH** with the complexes **S4**−**S6** derived from **1-(H_2O)**, we see that binding of urea discriminates between these models. The key observation here is that inclusion of urea as a nickel ligand in the **S1B** and **S3** structures is clearly compatible with catalysis through the nucleophilic addition of W2 or WB to the urea carbonyl group, whereas none of the complexes **S4**−**S6** exhibit geometries favorable for nucleophilic attack.

Mechanism A: Hydrolysis of Urea Starting from the Bidentate Urea-Bound Complex S3. According to the available mechanistic proposals, the hydrolysis of urea by the ureases would start at a bidentate complex formed between urea and the nickel ions in which the bridging hydroxide would attack the carbonyl C atom of urea to give a tetrahedral intermediate. Subsequently, the bridging hydroxide group would donate an H atom to the leaving ammonia molecule as proposed by Benini et al..[10] Alternatively, the required proton could be donated by the general acid His320 (*K. aerogenes* numbering) as proposed by Karplus et al..[13] In this scenario, the complex **S3** represents the first critical structure along the reaction coordinate from which a tetrahedral intermediate could be readily formed.

At this point, it is interesting to briefly analyze how **S3** fits into the active site of urease. We docked the **S3** structure into the 1FWJ crystal structure of *K. aerogenes* urease (see Figure 6). In the 1FWJ model, the flexible flap of residues is in the "closed" conformation, which is thought favorable for catalysis. Despite the qualitative nature of our docking analysis, the relative orientation of urea fits the protein environment and allows stabilizing interactions with nearby residues. In particular, the carbonyl group of urea can hydrogen bond with the His219 side chain while one of the amino groups can interact with the main chain carbonyl of Ala167. The second amino group can be stabilized by the main chain carbonyl groups of Ala363 and Gly277 and the imidazole ring of His320 (see Figure 6).

By carrying out QM calculations on the dinickel cluster models, we modeled the conversion of **S3** into a tetrahedral

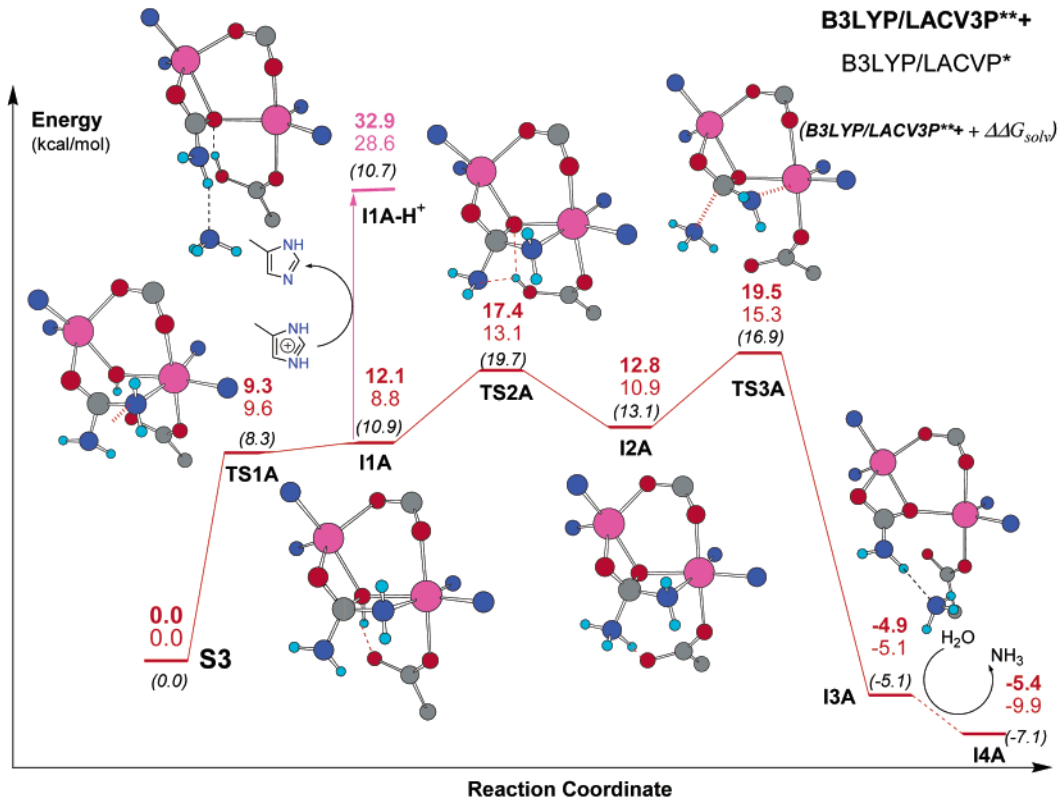

Figure 7. Energy profile along the reaction mechanisms for the hydrolysis of urea starting at the bidentate (**S3**) complex. Relative energies at various levels of theory with respect to **S3** are in kcal/mol. For the sake of clarity, only selected atoms are represented in the ball-and-stick models.

intermediate. From the tetrahedral intermediate, two pathways for the proton transfer to the leaving ammonia were investigated: (1) an intramolecular process in which the WB hydroxide donates its proton to one amino group; (2) an intermolecular process in which the proton would come from a protonated methyl-imidazole mimicking a histidine side chain. For the second alternative, we only studied its energetics in the context of the gas phase or in continuum solvent. The resultant energy profile and all the critical structures (transition states and intermediates) located on the B3LYP/LACVP* PES are represented in Figures 7 and 8. The most relevant equilibrium distances of the reactive bonds are collected in Table S5 in the Supporting Information.

The transition state (TS) for nucleophilic attack, **TS1A** in Figure 7, corresponds to a *late* TS since the C(urea)—O(WB) bond is quite advanced (1.795 Å). Simultaneously, the C═O and C—N bonds in the urea moiety are elongated while the Ni1—O and Ni2—N distances decrease in **TS1A** with respect to the precursor complex **S3**. The B3LYP/LACV3P**+ energy barrier amounts to 9.3 kcal/mol relative to **S3**. The tetrahedral intermediate corresponds to the structure **I1A** which is 0.8 kcal/mol below **TS1A** at the B3LYP/LACVP* level. Thus, **I1A** is very close to **TS1A** both in energy and in geometry. In fact, single-point B3LYP/LACV3P**+ energy calculations indicate that **I1A** is higher in energy than **TS1A** by 2.8 kcal/mol; hence, **TS1A** would not be a true transition state, and the tetrahedral intermediate would not exist at higher levels of theory. In other words, nucleophilic attack of the WB hydroxide on urea in the **S3** complex could lead to a tetrahedral intermediate that is only transiently stable.

Regardless of its likely transient character, **I1A** constitutes an appropriate starting point to study the mechanism of subsequent proton transfers. For example, the H-bond contact between the WB hydroxide and the Oδ2 atom of the Ni2-bound carboxylate is quite short in **I1A** with an O···O distance of 2.455 Å. This suggests that, in effect, WB could donate its proton with the assistance of the carboxylate group as proposed by Benini et al. On the other hand, the noncoordinated amino group in **I1A** could well accept the proton from WB or another acid group (when the structure of **I1A** is docked in the 1FWJ active site, the N···N separation between the amino group of urea and the Nϵ2@His320 atom is 3.7 Å). We first considered proton donation by an acid. Thus, a proton was attached to the free amino group in **I1A**, and the complex **I1A**—$\mathbf{H}^+$ was obtained (see Figure 7). As observed from the equilibrium geometry of **I1A**—$\mathbf{H}^+$, protonation of **I1A** by a generic acid provokes a large structural rearrangement. An ammonia molecule is released from the dinickel cluster, the Ni2-bound carboxylate becomes protonated, the Ni2—N bond is broken, and a planar carbamate moiety is formed. In **I1A**—$\mathbf{H}^+$, the carbamate anion binds to Ni1 in a bidentate manner and, simultaneously, one of its O atoms (the original O atom of WB) bridges Ni1 and Ni2.

To find out if protonation of **I1A** by an acid group is energetically favorable, we computed the gas-phase reaction energy for the acid—base process shown in Scheme 3, where the methyl-imidazolium/methyl-imidazole pair somehow mimics the action of the proposed general acid in urease catalysis. The corresponding energy change amounts to 20.8 kcal/mol; that is, protonation of **I1A** by mehtyl-imidazolium is quite unfavorable in the gas phase. In the energy profile shown in Figure 7, **I1A** is connected to the **I1A**—$\mathbf{H}^+$ structure by protonation, **I1A**—$\mathbf{H}^+$ being 32.9 kcal/mol above the energy origin at **S3**. We conclude that the intrinsic basicity of **I1A** as compared with that of methyl-imidazole is rather low. However, we must note

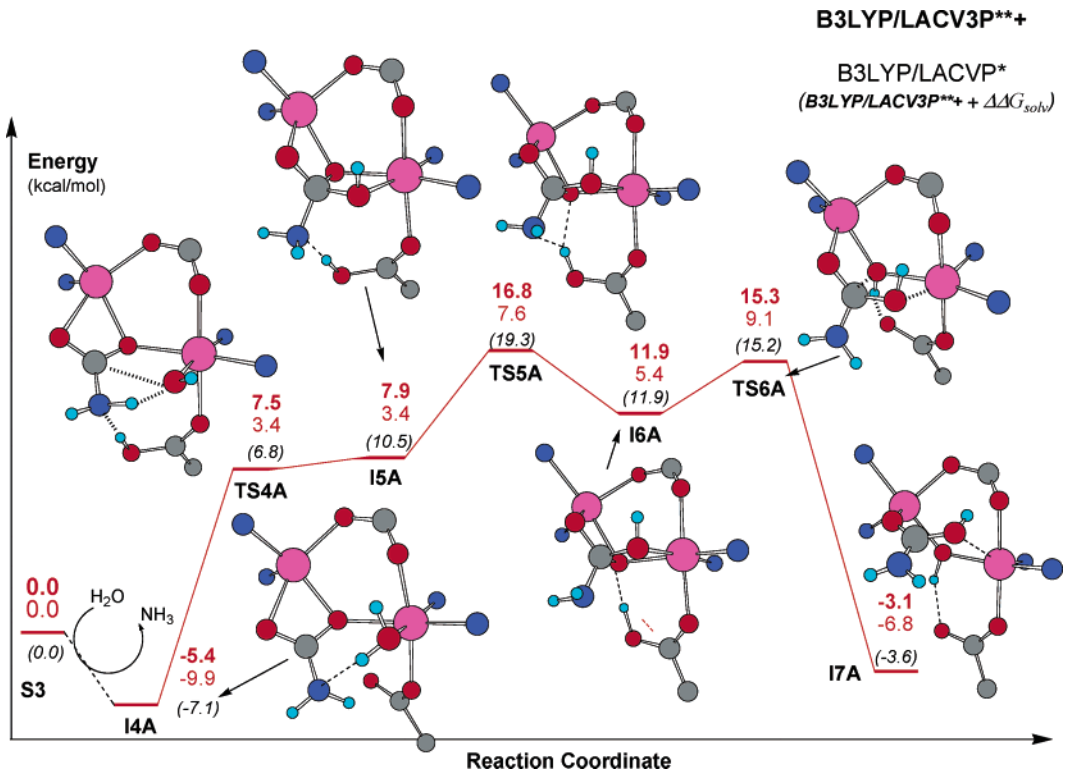

Figure 8. Energy profile along the reaction mechanism for the release of carbamic acid starting at the intermediate structure (**I4A**). Relative energies at various levels of theory with respect to **S3** are in kcal/mol. For the sake of clarity, only selected atoms are represented in the ball-and-stick models.

Scheme 3

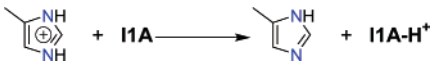

that environmental effects may have a large effect on the energetics of the protonation process. For example, addition of the ΔG_{solv} terms estimated by single-point PB SCRF B3LYP/LACVP* calculations to the gas-phase energies results in a slightly exothermic energy (−0.2 kcal/mol) for the acid−base process shown in Scheme 3. In other words, an environment with a high dielectric constant might favor the participation of an external imidazole group. Nevertheless, it is also clear that a more definitive assessment about the participation of an acid in the catalytic process of ureases will need to take into account the heterogeneous protein and aqueous environment surrounding the dinickel clusters.

The second possibility for the proton transfer in **I1A** proceeds through the intramolecular process characterized by the series of structures **I1A** → **TS2A** → **I2A** → **TS3A** → **I3A** (see Figure 7). According to our calculations, **TS2A** is a transition state for the 1,3-H transfer from the hydroxide fragment (WB) to the free amino group in **I1A**. Most interestingly, the proton being transferred in **TS2A** is bound to the Oδ2 atom of the carboxylate group (O−H = 1.000 Å) and establishes a bifurcated H-bond with the donor and acceptor atoms (O(WB)···H = 1.932 Å; N···H = 2.106 Å). The stabilizing effect of the carboxylate group on the in-flight proton allows this process to occur with a low energy barrier. Thus, **TS2A**, which is only 5.3 kcal/mol above **I1A**, has an energy barrier of 17.4 kcal/mol in the gas phase with respect to the initial bidentate structure **S3**.

Completion of the proton transfer from **TS2A** leads to the intermediate **I2A** in Figure 7. **I2A** is now 4.6 kcal/mol more stable in the gas-phase than its precursor transition state **TS2A** and 12.8 kcal/mol less stable than **S3**. Structurally, **I2A** is a tetrahedral intermediate similar to **I1A**, which maintains the same coordination to the nickel ions. In **I2A**, the proton originally bound to the WB oxygen atom is shared between the carboxylate group and the leaving ammonia molecule through a short hydrogen bond (N···O = 2.497 Å) with the proton lying at 1.277/1.228 Å from the N/O ends. With respect to **I1A**, the C−N bond of the free amino group elongates from 1.430 Å to 1.530 Å.

From **I2A**, the next mechanistic step involves the expulsion of the ammonia molecule. At the corresponding transition state, **TS3A**, the estimated transition vector is dominated by the elongation of the breaking C−N bond, which is 1.972 Å long. The calculated energy barrier for **TS3A** amounts to 19.5 kcal/mol, 2.1 kcal/mol above the TS for the 1,3-H shuttle **TS2A**.

From **TS3A**, the minimum energy structure located on the B3LYP/LACVP* PES is **I3A** in Figure 7. In **I3A**, the coordination sphere around Ni2 has an empty equatorial position, the planar NH_2−COO^- moiety binds to Ni1 through its carboxylate group and also maintains the Ni1···Ni2 bridge, the formed ammonia molecule is bound to the carbamate fragment and the carboxylate group by typical H-bond contacts, and so forth. Thus, the complex **I3A** resembles the structure **I1A**−$\mathbf{H}^+$. However, **I3A**, which is formed via intramolecular proton transfer from WB, is energetically much more stable in the gas phase by 37.8 kcal/mol than the **I1A**−$\mathbf{H}^+$ structure that results from the acceptance of a proton from an external methylimidazolium acid. This energy difference decreases to 15.8 kcal/mol when the PB-SCRF solvation energies in aqueous solution are considered.

Presumably, ureases release carbamic acid and ammonia with a simultaneous binding of water to the nickel ions in order to regenerate the active site for the next turnover. To investigate these reaction events along the intramolecular pathway **A**, we optimized one more intermediate structure, **I4A** in Figures 7 and 8, in which the ammonia molecule originally present in **I3A** is replaced by an Ni2-bound water molecule, which occupies an equatorial binding position. According to our calculations, the **I3A** + H_2O → **I4A** + NH_3 process is slightly exothermic in the gas phase by −0.5 kcal/mol at the B3LYP/LACV3P**+//B3LYP/LACVP* level.

Interestingly, the Ni2-bound water molecule (W2) at **I4A** is well situated for donating one H atom to the N atom of the carbamate moiety and subsequently attacking the C sp^2 atom (the corresponding O(W2)···N(carbamate) and O(W2)···C(carbamate) distances at **I4A** are 2.91 and 3.04Å, respectively). Indeed the series of structures **I4A** → **TS4A** → **I5A** → **TS5A** → **I6A** → **TS6A** → **I7A** shown in Figure 8 describes a mechanism through which the W2 molecule reacts with the carbamate moiety to give a neutral carbamic acid molecule and to simultaneously regenerate the Ni1−OH−Ni2 bridge. First, the **I4A** complex passes through the transition state representing the nucleophilic attack of W2 (**TS4A**) to give a tetrahedral intermediate (**I5A**) in which W2 is bound to the carbamate moiety. Ongoing from **I4A** to **TS4A**, the N atom of the carbamate moiety acts as a bifunctional catalyst by accepting an H atom from the attacking W2 molecule and releasing a second H atom to the Ni2-bound acetate fragment. The two structures, **TS4A** and the tetrahedral intermediate **I5A**, are nearly isoenergetic on the B3LYP/LACVP* PES, with both being ∼13 kcal/mol above the **I4A** complex. However, **I5A** is 0.4 kcal/mol above **TS4A** in terms of the B3LYP/LACV3P**+ energies, and hence, **I5A** is likely only transiently stable. The evolution of **I5A** toward the formation of carbamic acid proceeds through a TS involving rearrangement of H-bonds (**TS5A**). In **TS5A**, the hydroxyl group of the Ni2-liganded acetic acid breaks its OH···N contact with the carbamic moiety in **I5A** to give a shorter H-bond with the Ni1···Ni2 bridging O(WB) atom in **I6A** (see Figure 8). The transition structure **TS5A** has an energy barrier of 22.2 kcal/mol with respect to **I4A** and is 16.8 kcal/mol above **S3**. Finally, protonation of the Ni1···Ni2 bridging O(WB) atom by the Ni2-bound carboxyl group turns out to be the trigger event for the release of the carbamic acid molecule from the tetrahedral intermediate **I6A** (see Figure 8). The corresponding TS, **TS6A**, which is 20.7 kcal/mol above the **I4A** complex, leads to a quite stable complex **I7A**, which is only 2.3 kcal/mol less stable in the gas phase than **I4A**. The **I7A** structure corresponds to a monodentate adduct between the carbamic acid molecule and the dinickel cluster with the Ni1−OH−Ni2 bridge. The overall energy change for the **I7A** + 3 H_2O → **1-OH** + NH_2−COOH process is exothermic by −22.4 kcal/mol at the B3LYP/LACV3P**+//B3LYP/LACVP* level. This exothermicity stems from the formation of the Ni−water bonds (the hydrolysis of urea to yield carbamic acid and ammonia has a calculated ΔE of only −2.1 kcal/mol).

Clearly, the large series of structures shown in Figures 7 and 8 reveal many molecular details of the intramolecular pathway for the catalytic hydrolysis of urea bound to the nickel centers in a bidentate manner. Of course, in this mechanism, the role played by the Ni1···Ni2 bridging hydroxide (WB) is of particular interest: WB acts initially as the nucleophile (**TS1A** and **I1A**) attacking the urea molecule to give one ammonia molecule and a carbamate anion (NH_2−COO^-) which bridges Ni1 and Ni2. However, a second water molecule (W2), which binds to the Ni2 center once the ammonia molecule is released, also plays a crucial role in this mechanism by attacking the carbamate anion to finally release a carbamic acid molecule and regenerate the dinickel complex. Remarkably, the Ni1−WB−Ni2 bridge is conserved all along the reaction profile. Our calculations predict that, in the gas phase, the rate-determining step would be the release of the ammonia molecule at **TS3A** with an energy barrier of 19.2 kcal/mol with respect to the bidetante complex **S3**. However, other transition structures (e.g., **TS2A** for 1,3-H transfer assisted by the Ni2-bound carboxylate group) are only ∼2−3 kcal/mol below **TS3A**, and therefore, a definite prediction on the nature of the rate-determining TS in mechanism **A** is not possible at this time. Similarly, environmental effects could change the relative stability of the different TSs. In this respect, our PB-SCRF calculations suggest that **TS3A** can be stabilized by the environment, whereas **TS2A** is destabilized (see Figure 7). However, the PB-SCRF calculations also indicate that the energy profile for mechanism **A** does not depend dramatically on the environment polarity.

Mechanism B: Hydrolysis of Urea Starting from the Monodentate Urea-Bound Complex S1B. Although Karplus and co-workers have considered that the bridging WB is the most likely candidate to be the nucleophile in the catalytic mechanism of the ureases, they have not entirely ruled out that the Ni2-bound W2 molecule might be the hydrolytic water.[13] In fact, the structure and energetics of the monodentate complex **S1B** give support to this alternative mechanistic proposal since W2 in **S1B** is well positioned to be activated by WB and to attack the urea carbonyl group coordinated to the Ni1 center. To further investigate this mechanism, we carried out rigid docking analyses of the **S1B** structure within the 1FWJ and 2UBP crystal structures which have the "closed" and "open" conformations of the active site flap, respectively. When **S1B** is embedded within the 1FWJ structure, the Ni1-coordinated urea molecule shows two important steric clashes with the Ala167 carbonyl group and the side chain of His320. Thus, the "closed" conformation of the active site flap appears incompatible with the formation of monodentante complexes such as **S1B**, while the bidentate complex **S3** fits nicely within the 1FWJ structure (see above). However, when the "open" conformation is considered in the docking analyses, the resulting complex is much less impeded (see Figure 9). In this case, only the carbonyl group of Ala170 (*B. pasteurii* numbering) has a bad contact with one of the amino ends of urea, although this steric hindrance can be largely avoided by rotation around the Ni1−O(urea) bond. On the other hand, the side chain of His222 is well positioned to interact with the carbonyl group of urea. Although the protein flexibility and solvent dynamics must be considered to fully characterize urea-binding interactions, these results suggest that either **S1A**- or **S1B**-like structures could be possible if the active form of the enzyme has the "open" conformation.

According to our calculations, the hydrolysis of urea starting at the **S1B** complex can take place via a simple two-step mechanism, which involves a tetrahedral intermediate. The corresponding B3LYP/LACVP* critical structures are shown

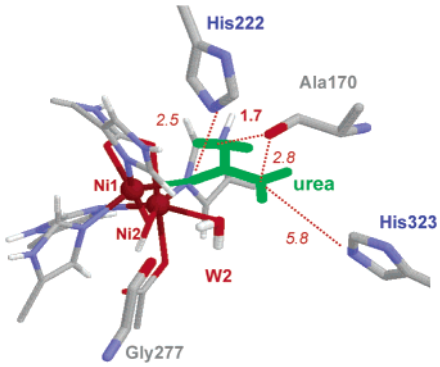

Figure 9. Docked structure of the prereactive complex **S1B** within the 2UBP X-ray structure (*B. pasteurii* residue numbering). Protein atoms were held fixed, and the side chains of the residues liganded to the nickel ions were replaced by the QM atoms. Select distances are given in Å.

in Figure 10, while some important equilibrium distances are collected in Table S6 in the Supporting Information.

From the prereactive complex **S1B** to the transition state connecting to the tetrahedral intermediate (**TS1B**), the nucleophilic W2 becomes activated by WB, the urea molecule rotates around the Ni1−O(urea) bond in order to hydrogen bond with WB, and the forming C(urea)−O(W2) bond has a distance of 2.279 Å. The energy barrier of **TS1B** with respect to **S1B** is 31.5 kcal/mol in the gas phase. The proton being transferred, which is bound to the O atom of WB (O−H = 0.994 Å), forms a bifurcated hydrogen bond with the donor and acceptor atoms (O(W2)····H = 2.383Å; N(urea)····H = 1.807 Å). Thus, WB plays a critical role at **TS1B** by activating W2 and stabilizing the proton "in flight" similar to that of the Ni2-bound carboxylate group in the transition structure (**TS2A**) for the 1,3-proton transfer in mechanism **A**. From **TS1B**, completion of nucleophilic attack and proton transfer to the leaving N atom leads to the tetrahedral structure **I2B** in which a *zwitterionic* moiety (ammonia + carbamic acid) acts as a bidentate ligand bridging the Ni1 and Ni2 centers. This intermediate, which is only 2.7 kcal/mol below **TS1B**, next releases ammonia via the second transition structure (**TS2B**), which is very close to **I1B** both structurally and energetically. At **TS2B**, the rupture of the C−N bond (1.911 Å) is accompanied by the elongation of the Ni2−O(carbamic acid) bond (2.368 Å) since the metal−ligand ability of the *neutral* carbamic acid is lower than that of its *zwitterionic* complex with ammonia. Thus, at the product complex **I2B**, the carbamic acid is coordinated only to Ni1 via its carbonyl group, the ammonia molecule being placed at the second ligand shell around the Ni1. In terms of the computed relative energies, **I2B** is 0.9 kcal/mol less stable than the initial complex **S1B**. Concerning the effects of the environment polarity on this reaction mechanism, all the critical structures are equally destabilized by ∼4−5 kcal/mol with respect to the bidentate complex **S3.** However, the relative energies of **TS1B**, **I1B**, and **TS2B** with reference to their precursor complex **I1B** are only slightly altered by ±0.5 kcal/mol (see Figure 10).

Comparison between Mechanisms A and B. The energy profiles corresponding to the mechanisms **A** and **B** are represented in Figures 7−8 and 10, respectively, the relative energies being given with respect to the complex **S3**. In these figures, we see that the rate-determining transition structures for both mechanisms (i.e., **TS3A** and **TS1B**) are very close in energy when a common energetic reference is considered (∼19 kcal/mol above **S3**). Inclusion of the PB-SCRF solvation energies favors preferentially the mechanism **A** by around 4 kcal/mol. We note, however, that a clear assignment of which mechanism should be the most favorable one in the active site ureases cannot be obtained from the results of our QM calculations on cluster models.

Besides the QM energy profile, we can also compare both mechanistic pathways on the basis of docking analyses. As shown in Figure 6, the formation and subsequent evolution of the bidetante complex **S3** may be stabilized by several specific

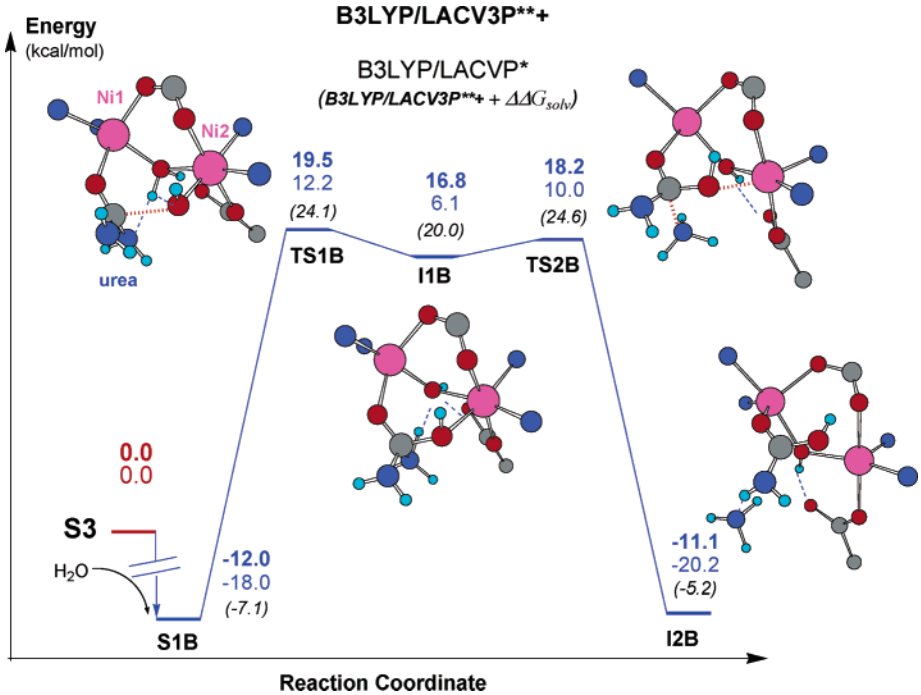

Figure 10. Energy profile along the reaction mechanisms for the hydrolysis of urea starting at the monodentate (**S1B**) complex. Relative energies at various levels of theory with respect to **S3** are in kcal/mol. For the sake of clarity, only selected atoms are represented in the ball-and-stick models.

residue-urea interactions, which may be present when the active site adopts the "closed" conformation. A similar observation has been found in previous docking calculations.[24] Thus, it seems that the mechanism **A**, which basically corresponds to that proposed by Benini et al.,[10] could be favored preferentially by the protein environment. However, it must be noted that the alternative mechanism **B** in which the Ni2-bound water molecule attacks the Ni1-coordinated urea might be viable in the "open" state of the active site. It may also be interesting to note that mechanism **B** is much "simpler" than **A**: while product release from **I2B** can occur easily via water exchange processes at the Ni1 center without altering the Ni1−OH−Ni2 motif, the regeneration of the catalytic dinuclear complex in mechanism **A** takes place through a ligand exchange process at Ni2, followed by a water nucleophilic attack to the carbamate moiety and proton-transfer steps prior to the expulsion of a carbamic acid molecule.

Clearly, further theoretical work oriented toward computation of free energy profiles and taking into account the solvated active site of ureases will be required in order to definitively determine the relative energy difference between mechanism **A** (WB and W2 = nucleophiles) and **B** (W2 = nucleophile) as well as to provide accurate activation parameters. These simulations should also include entropic contributions arising from the structural elasticity of the ureases in order to obtain a deeper understanding of the origin of the high catalytic proficiency exhibited by the ureases (e.g., *K. aerogenes* urease has a k_{cat} value of 3500 s^{-1} [1]). Nevertheless, it is tempting to speculate herein that both mechanisms might have similar ΔG barriers in the enzyme so that both conformational states of the active site, "closed" and "open", might be catalytically productive.

Summary and Conclusions

In this work, we employ computational methodologies to characterize a family of dinickel complexes that are relevant to the catalytic hydrolysis of urea exerted by the urease enzymes. The analyses of the equilibrium geometries, electronic properties, and energies for a series of realistic complexes modeling the urease active site gave new insights into the structure, substrate binding, and catalytic mechanism of these important nickel-containing enzymes. In addition, the QM model complexes provide geometries, relative energies, charge distributions, reaction pathways, and so forth, which form a foundation for further investigations of the ureases using complimentary methodologies (QM/MM, MM, linear scaling QM, etc.).

Concerning the structure of the native form of the ureases enzymes, the most interesting results and conclusions obtained from our calculations on cluster models are as follows:

(1) Neither water-bridged nor oxo-bridged structures correspond to stable minima on the PES. Therefore, the Ni1−WB−Ni2 motif in the crystallographic structures is safely assigned as a hydroxide bridge.

(2) Two different protonation states represented by the **1-OH** (unprotonated Asp) and **1-(H_2O)** (neutral Asp) with global charges of +1 and +2, respectively, show very similar structural and magnetic properties according to our calculations. This suggests that the coordination environment of the Ni ions in the active site would be stable against variations of pH.

(3) In our calculations, both the carbamylate bridge and the hydroxide bridge connecting the Ni ions are quite stable. Hence, the dinuclear complex is basically *rigid* having an Ni1···Ni2 separation of around 3.5−3.6 Å.

From the urea-complexed models, we conclude the following:

(4) Urea can give both monodentate adducts with retention of the Ni2-bound water molecule and bidentate adducts. Our calculations indicate that other factors (entropy, specific residue-urea contacts, desolvation of the active site, etc.) will provide the driving force for urea binding since the nickel−urea bonds are less stable than nickel−water bonds.

(5) Either the configuration with negatively charged Asp or the neutral Asp form can bind the urea substrate; that is, urea binding would not be pH dependent. However, in our calculations, prereactive complexes in which urea binds with a favorable orientation for catalysis have a negatively charged Asp. Hence, we propose that the configuration with unprotonated Asp would correspond to the kinetically active configuration of the enzyme.

(6) Complex **S3**, in which urea binds in a bidentate manner, resembles the crystallographic structure of the DAP-inhibited urease enzyme from *B. pasteurii*. This structure, which fits well to the "closed" conformation of the active site, strongly suggests that the Ni1···Ni2 bridging hydroxide can act as the nucleophile.

(7) The characterization of complex **S1B**, in which urea binds to the Ni1 center, suggests that an Ni2-bound water molecule could be activated by the bridging hydroxide. The docking analyses indicate that this mechanism would only be possible in the "open" conformation of the active site.

From our calculations on the reaction mechanisms starting at **S3** (mechanism **A**) and **S1B** (mechanism **B**), several mechanistic implications can be outlined:

(8) For mechanism **A**, the Ni1−WB−Ni2 motif is conserved all along the reaction profile.

(9) In mechanism **A**, WB acts initially as the nucleophile attacking the urea molecule to give one ammonia molecule and a carbamate anion bridging the Ni1 and Ni2 ions. Subsequently, one water molecule binds to the empty coordination site at Ni2 and attacks the carbamate anion to release carbamic acid, thereby, regenerating the dinickel complex.

(10) For mechanism **A**, protonation from an external acid in the gas phase is not a competitive mechanism, whereas the proton transfer from WB to the leaving N atom is clearly viable with the assistance of the carboxylate group of the Ni2-bound Asp.

(11) For mechanism **B**, formation of carbamic acid and ammonia occurs in a two-step mechanism in which the WB hydroxide plays a crucial role to shuttle one H atom from the water molecule W2 to the leaving N atom.

(12) The stability of the rate determining TSs for both mechanisms **A** and **B** is similar. Moreover, both the Ni1···Ni2 bridging WB and the Ni2-bound W2 molecules play active kinetic roles during the two mechanisms **A** and **B**.

(13) The stationary points located for the two mechanisms give a rationale for the presence of a *dinickel* active site in the ureases. In all the structures, the Ni1···Ni2 separation is very similar (3.5−3.6 Å) and the two metal ions preserve their coordination spheres (squared-pyramidal and octahedral). Thus, the relatively rigid and stable coordination environment around the nickel(II) ions (as opposed to the higher kinetic lability and lower thermodynamic stability of zinc(II) complexes) ensures

that a small urea molecule can bind in either bidentate or monodentate fashion with the precise orientation necessary for catalysis.

Acknowledgment. We thank the NIH via Grant GM066859 for supporting this research project and National Center for Supercomputer Applications (NCSA) for generous allocations of supercomputer time.

Supporting Information Available: Energies and nickel−ligand bond distances for all the small complexes Ni−L and Ni−L−Ni. Figures showing the structure, spin density, and atomic charges for the small complexes $[NiOHNi]^{3+}$ and $[NiONi]^{2+}$. Figures showing the B3LYP/LACVP* optimized structures of all the dinickel complexes including NPA charges of the nickel ions and nickel−ligands. Selected distances and energies of all the dinickel complexes (24 pages, print/PDF). Cartesian coordinates of the B3LYP/LACVP* optimized structures in CIF format. This material is available free of charge via the Internet at http://pubs.acs.org.

JA030145G